


Review

Pump-Probe Time-Resolved Serial Femtosecond Crystallography at SACLA: Current Status and Data Collection Strategies

Eriko Nango ^{1,2,*} , Minoru Kubo ^{3,*}, Kensuke Tono ^{2,4} and So Iwata ^{1,2}

¹ Department of Cell Biology, Graduate School of Medicine, Kyoto University, Yoshidakonoe-cho, Sakyo-ku, Kyoto 606-8501, Japan; s.iwata@mfour.med.kyoto-u.ac.jp

² RIKEN SPring-8 Center, 1-1-1, Kouto, Sayo-cho, Sayo-gun, Hyogo 679-5148, Japan; tonos@spring8.or.jp

³ Graduate School of Life Science, University of Hyogo, Kouto 3-2-1, Kamigori-cho, Ako-gun, Hyogo 678-1297, Japan

⁴ Japan Synchrotron Radiation Research Institute, 1-1-1 Kouto, Sayo, Hyogo 679-5198, Japan

* Correspondence: e.nango@mfour.med.kyoto-u.ac.jp (E.N.); minoru@sci.u-hyogo.ac.jp (M.K.)

Received: 12 November 2019; Accepted: 12 December 2019; Published: 14 December 2019



Abstract: Structural information on protein dynamics is a critical factor in fully understanding the protein functions. Pump-probe time-resolved serial femtosecond crystallography (TR-SFX) is a recently established technique for visualizing the structural changes or reactions in proteins that are at work with high spatial and temporal resolution. In the pump-probe method, protein microcrystals are continuously delivered from an injector and exposed to an X-ray free-electron laser (XFEL) pulse after a trigger to initiate a reaction, such as light, chemicals, temperature, and electric field, which affords the structural snapshots of intermediates that occur in the protein. We are in the process of developing the device and techniques for pump-probe TR-SFX while using XFEL produced at SPring-8 Angstrom Compact Free-Electron Laser (SACLA). In this paper, we described our current development details and data collection strategies for the optical pump X-ray probe TR-SFX experiment at SACLA and then reported the techniques of in crystallo TR spectroscopy, which is useful in clarifying the nature of reaction that takes place in crystals in advance.

Keywords: X-ray free-electron laser; time-resolved crystallography; pump-probe experiment; microcrystals

1. Introduction

X-ray crystallography is a powerful tool for determining the protein structure at high spatial resolution. To date, atomic structural information has been valuable in elucidating the mechanisms and designing pharmaceuticals, because of the close relation between the tertiary structure of proteins and their functions. In general, the tertiary structure of proteins at work changes from the initial structure before a reaction; however, it remains a challenge that conventional X-ray crystallography captures protein dynamic structures. The Laue method with polychromatic synchrotron X-rays [1] or cryotrapping to capture intermediates at cryogenic temperatures has so far been used to observe the active state in which a protein functions. Nevertheless, there is a limit for which samples can be applied to the Laue method due to technical difficulties. For instance, there is a tendency for crystals to suffer from radiation damage that is caused by X-rays from synchrotron radiation sources, which results in artificial structural changes in proteins. Moreover, protein reactions may proceed, even at cryogenic temperatures, and cause changes that vary from time-dependent changes upon a reaction initiator, such as photoexcitation. Indeed, the determination of protein dynamic structures at atomic resolution has been one of the hefty challenges in structural biology for quite a long time.

X-ray free-electron lasers (XFELs) produce intense, ultrashort pulses; as such, XFELs have enabled room-temperature protein structure determination via diffraction patterns from microcrystals before any manifestation of radiation damage [2]. Furthermore, these femtosecond X-ray pulses from XFEL can capture rapid structural changes in proteins to allow for the visualization of the dynamic process in proteins at atomic resolution. Hence, serial femtosecond crystallography (SFX) is a recently established method for protein structure determination by XFEL [3,4]. In SFX, the microcrystals are continuously delivered into an intersection point with an XFEL beam, because the preceding XFEL pulse destroys the samples. Subsequently, intense X-ray pulses afford still diffraction patterns from randomly oriented microcrystals, which results in a protein tertiary structure in a condition close to physiological temperature.

In Japan, the SPring-8 Angstrom Compact Free-Electron Laser (SACLA) started user operations in 2012 [5] after the Linac Coherent Light Source (LCLS) in the USA [6]. A consortium of researchers from structure biology, physics, engineering, and XFEL science was organized in 2012 for an SFX project named “Rapid Structure Determination System for Drug-target Proteins Using the X-ray Free Electron Laser” that was directed by Prof. So Iwata under the X-ray Free-Electron Laser Priority Strategy Program of the Ministry of Education, Culture, Sports, Science & Technology in Japan (MEXT). The project established the foundation of devices and techniques for SFX at SACLA for the first five years. This foundation has also led to the development of a setup for pump-probe time-resolved serial femtosecond crystallography (TR-SFX), which uses a pump laser pulse to trigger reactions. In 2015, the first experiment of pump-probe TR-SFX at SACLA was conducted while using a light-driven proton pump, bacteriorhodopsin (bR), and, in early 2016, we succeeded in observing the structural changes in bR during proton transfer at thirteen-time points from nanoseconds to milliseconds subsequent to light excitation while using a pump laser [7]. The result was the first three-dimensional movie of large structural changes throughout a protein, which reveals how such structural changes in bR achieve unidirectional proton transport across the membrane. Pump-probe TR-SFX techniques have been further applied to various proteins, including photosystem II (PSII), which is a huge membrane-protein complex that catalyzes light-driven water oxidation at its catalytic center [8]. Suga and coworkers achieved an observation of structural changes in PSII induced by two-flash illumination, which provided insight into the mechanism of the O=O bond formation in the catalytic center. Additionally, we conducted the first successful TR-SFX study while using a caged compound to capture the enzymatic reaction in a fungal NO reductase [9].

Here, we introduce the device development and data collection strategy for the pump-probe TR-SFX experiments at SACLA. We also describe in crystallo TR spectroscopy to assess the structural dynamics in the crystalline phase, which should be performed before conducting TR-SFX. Our data collection strategy helps to efficiently acquire good data of TR-SFX during the limited beamtime of XFEL.

2. Pump-Probe Time-Resolved SFX Experiments

The pump-probe technique for TR-SFX has been well established for the past five years. Here, optical pulses (“pump”) illuminate a continuous flow of protein microcrystals, followed by the XFEL pulses (“probe”) illuminating with various delay times to obtain time-resolved (TR) diffraction images. The important applications of this technique include direct observations of structural changes in photosensitive proteins. In general, relatively large movements in a protein, such as helix movements, occur in microsecond- and millisecond-timescales, while local motions in a protein, such as photoisomerization of a chromophore, proceed on the ultrashort timescale of femtoseconds to picoseconds [10].

The first experiment of time-resolved SFX was conducted in 2012 while using an optical pump laser that was synchronized with an XFEL of the LCLS to obtain X-ray diffraction images from the photoactivated state of a large membrane-protein complex [11]. In this experiment, photosystem I-ferredoxin co-crystals that were flowing in a liquid jet were irradiated with the optical pump laser

and then shot by the XFEL, which resulted in light-induced changes at time delays of 5 to 10 μ s. The combination of the liquid jet sample injector and an optical pump laser was also used for the early time-resolved SFX studies (photoactive yellow protein [12,13], myoglobin [14]). For instance, the trans-to-cis isomerization of the chromophore in photoactive yellow protein (PYP) was observed to arise at approximately a 590-fs time delay after photoexcitation [13], and the displacement of side chains in the chromophore pocket in PYP was observed to occur at a 1- μ s time delay [12]. These studies were performed at the Coherent X-ray Imaging (CXI) beamline of the LCLS [15], where the sample was delivered to an X-ray interaction point by a liquid jet injector in a vacuum chamber that was installed at the CXI. Data collection in a vacuum has the advantage of low background noise, as well as the avoidance of X-ray attenuation; however, evaporative cooling might cause temperature changes on a sample stream. Moreover, a vacuum environment offers less flexibility when installing devices, such as optics for a pump laser or a sample injector.

Meanwhile, a helium chamber was introduced for the SFX experiments at the beginning of user operation at SACLA [16]. Sample delivery in SFX requires a thin stream with a high density of microcrystals to ensure a high hit rate; however, it is prone to clogging the nozzle of an injector. A helium atmosphere environment allows for the easy replacement of an injector and provides more flexibility in setting devices when compared to a vacuum environment, thus facilitating SFX data collection [17]. This experimental setup (Diverse Application Platform for Hard X-ray diffraction In SACLA (DAPHNIS)), which consists of a helium chamber, a detector, an injector manipulator, and microscopes for the alignment of sample position, has been used for SFX experiments since 2013 [16]. In 2015, a new design of an experimental setup for pump-probe TR-SFX was adopted for achieving a high photoexcitation efficiency of samples and facilitating data collection. Figure 1 shows the recent setup for TR-SFX [18], which is composed of a pump-laser system, an injector manipulator, microscopes, and a multi-port readout charge-coupled device detector [19]. A nanosecond pump laser is incorporated into the setup to capture relatively large movements in proteins that occur at a delay time that is slower than nanoseconds. A pump-laser beam is divided into two arms while using a 50:50 beamsplitter, and each branch is fed into an optical fiber and then delivered near a sample stream. Each output beam from an optical fiber is collimated while using a fiber-coupled collimator and focused on a sample stream using an objective lens. The double-beam delivery system enables the illumination of protein crystals from two directions to enhance the excitation efficiency. Furthermore, optical fibers facilitate the pump beams' alignment procedure, because the pump beam paths from the laser to fiber inputs and from fiber outputs to the objective lenses are normally fixed. Two-types of pump-laser systems are currently available: an optical parametric oscillator (OPO) providing >1 mJ, 6 ns pulses at a wavelength that is tunable from 300 to 2000 nm with a repetition rate of up to 30 Hz (NT230, EKSPLA) and an Nd:YAG laser that delivers 12 mJ, 5 ns pulses at 532 nm with a repetition rate up to 15 Hz (Minilite-I, Continuum). The focal size of the pump beams is changeable from 20 μ m (FWHM) to 250 μ m (top-hat), depending on fiber core size (50–400 μ m). The pump beam can be spatially aligned with the XFEL beam while using XYZ stages controllable from outside of the experimental hutch. The pump laser is synchronized with the XFEL via a pulse generator (DG645, Stanford Research Systems), which can be used to easily adjust the delay time between the pump and XFEL pulses. The timing jitter is <1 ns when the delay time is set to <16.7 ms. When considering the pulse duration (6 ns) of the OPO laser, the time resolution is <7 ns. It should be noted that the timing jitter is approximately 0.1 ms for the delay time longer than 16.7 ms.

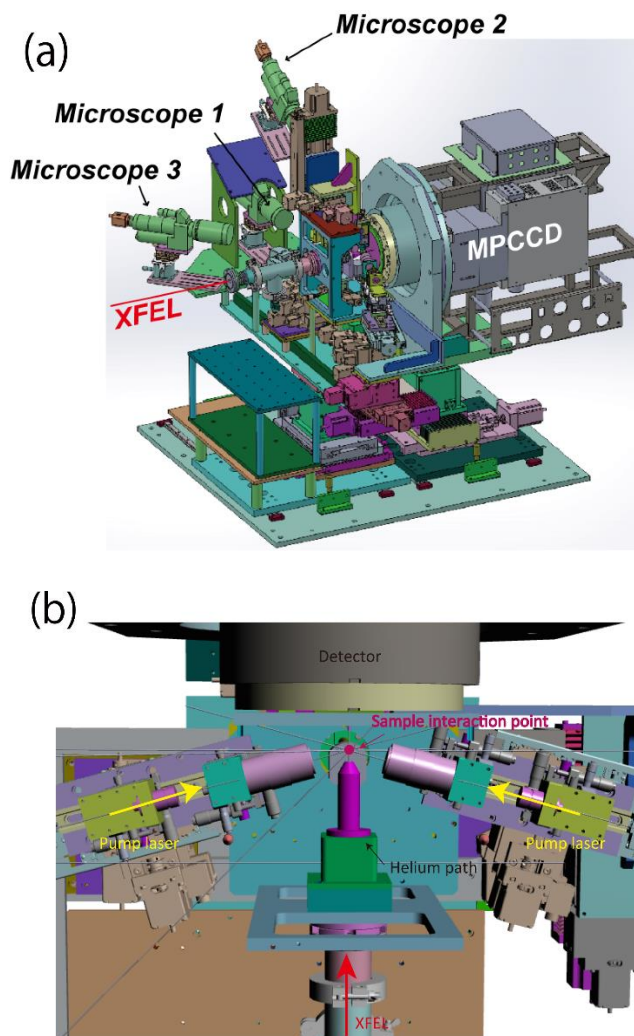


Figure 1. (a) Arrangement for pump-probe time-resolved serial femtosecond crystallography (TR-SFX) experiments using a nanosecond laser. An enlarged view around the sample interaction point is shown in (b).

A helium gas flow path, where a focused XFEL beam passes through, is introduced between the beamline exit and the sample position to reduce background noise from air scattering. Limited spaces around the sample cannot afford the use of a helium chamber. A sample is ejected from an injector that was mounted on a motorized manipulator and it is delivered to an XFEL focal point. A high-viscosity sample injector for ejecting viscous samples [20,21], such as crystals embedded in lipidic cubic phase (LCP) [22], is mainly used for the sample injection. Although a liquid jet injector, such as a gas dynamic virtual nozzle [23], is also applicable for sample delivery in pump-probe SFX, the available delay time is limited to within several microseconds, because the microcrystals that are illuminated by a pump laser flow down away from the intersection point with XFEL, basically due to its fast sample speed (approx. 10 m/s). A high-viscous sample can be delivered with a slow speed (approx. 10 mm/s), stretching the maximum delay to several tenths of ms, to overcome this problem. However, there are concerns regarding the instability of a high-viscous sample flow, which might cause inaccuracy in the delay time or multiple sample illumination.

In 2015, the developed setup for pump-probe TR-SFX was first demonstrated while using bR, which yields high quality microcrystals in LCP, with the Nd:YAG laser at a delay time (Δt) of 250 μ s after photoactivation to provide clear difference Fourier maps. After several experiments, the TR-SFX data were collected from the bR microcrystals after photoactivation for $\Delta t = 16$ ns, 40 ns, 110 ns, 290 ns,

760 ns, 2 μ s, 5.25 μ s, 13.8 μ s, 36.2 μ s, 95.2 μ s, 250 μ s, 657 μ s, and 1.725 ms at 2.1 angstrom resolution to provide 13 structural snapshots of conformational changes during proton transfer [7]. In the experiments, monoolein and paraffin oil were added into the bR microcrystals that were embedded in LCP before measurement to keep a stable flow from the highly viscous sample injector. In fact, the high-viscous mixture streams were recorded while using a high-speed camera to prove that the speed was stable (Figure 2). Moreover, Nogly et al. reported the viability of TR-SFX while using the LCP injector [20], with bR microcrystals in LCP at the beamline of the CXI at LCLS [24].

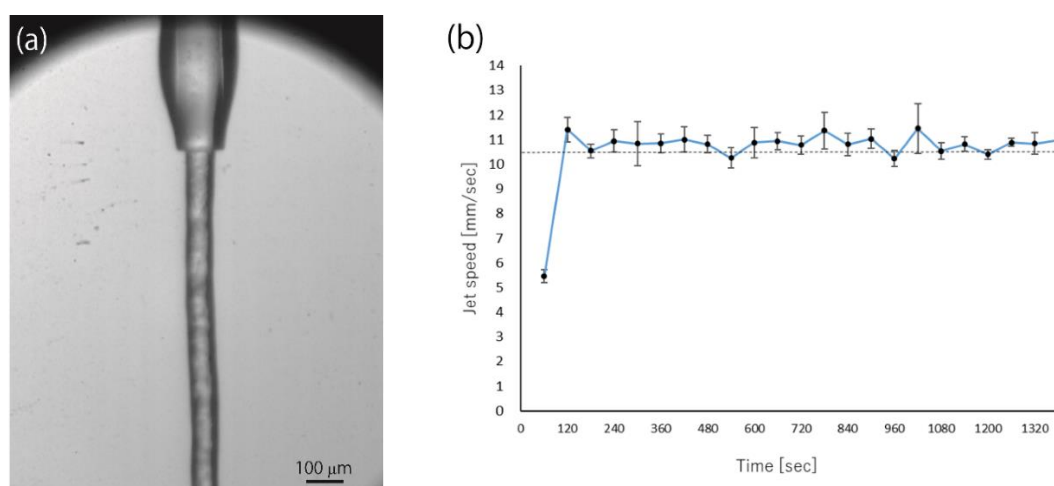


Figure 2. Jet speed measurements using high-speed imaging. (a) The photograph shows lipidic cubic phase (LCP) extrusion using the high-viscosity sample injector [21]. (b) Time course of LCP extrusion speed. Bacteriorhodopsin crystals embedded in the monoolein-based LCP were used for high-speed camera testing. The sample stream was recorded at 2000 frames per second using a high-speed camera (FASTCAM SA-Z). Three data points from each period of high-speed camera video (0.5 s of recording every 60 s) were plotted. The horizontal dotted line indicates that the target extrusion speed set via the high-performance liquid chromatography (HPLC) pump. Experimental condition: The sample, which was prepared according to the previous method [7], was extruded at a flow rate of 2.8 μ L/min as setting value of the HPLC pump from the nozzle with an inner diameter of 75 μ m using the high-viscosity injector [21]. A nitrogen sheath gas supplied from the outer nozzle of the injector was set to a flow rate of 0.7–1.0 L/min.

Other highly viscous carriers, such as grease [25] or hydroxyethyl cellulose [26], were also available for sample delivery in TR-SFX. The structural changes in PSII induced by two-flash illumination were observed at a resolution of 2.35 \AA while using the setup for TR-SFX at SACLA [8]. In this study, PSII microcrystals that were grown by a batch method were mixed with grease and injected by the high-viscosity sample injector. A hydroxyethyl cellulose matrix served for the TR-SFX of nitric oxide reductase (P450nor) with a caged substrate to capture the intermediate structures of the enzyme [9]. As such, this result defined the first successful experiment of TR-SFX while using a caged compound that releases a substrate by ultraviolet pump illumination at 308 nm.

Recently, not only the optical-fiber-based setup, but also different setups for the pump-probe experiments, have been developed. For instance, the femtosecond laser system [27] can be introduced into the pump-probe setup without optical fibers to trigger ultrafast reactions. For anaerobic samples, the DAPHNIS setup allows for sample injection in the helium chamber and illumination by a pump-laser pulse from one direction without using optical fibers. Additionally, a droplet injector generating pulsed droplets can be used for sample injection in pump-probe TR-SFX with smaller sample consumption than those with a liquid jet [28].

3. In Crystallo TR Ultraviolet-Visible Spectroscopy

The rate-limiting steps of protein reactions and, thus, the rates of intermediate formation and decomposition, generally depend on experimental conditions, such as temperature, pH, pressure, and solvent viscosity, among others. As such, the kinetics and detectable reaction intermediates in the crystalline phase are not necessarily identical to those in the solution phase. In this case, TR spectroscopy is useful in the evaluation of the in crystallo reaction kinetics. Thus, we performed TR visible absorption spectroscopy for bR microcrystals in the study of bR, which was key to the success of pump-probe TR-SFX.

Details of the visible microspectrometer were described previously [7,9]. In brief, the nanosecond, 532-nm pulse from an Nd:YAG laser (Minilite-I, Continuum) and the microsecond, white light pulse from a Xe-flash lamp were used as the pump and probe pulses, and they were both focused on the sample with Ø300 and Ø100 µm, respectively. The slurries of protein microcrystals were packed with a carrier medium (LCP in the case of bR) between two quartz windows with a 100-µm spacer and were then placed at the probe focal point. It should be noted that the microcrystal size of bR (typically, 20 µm) was smaller than the probe focal size, so that microcrystal ensembles, containing multiple microcrystals with random orientations, were measured. The sample cell temperature was kept at 20 °C with a water-cooled chiller.

Figure 3 shows the microsecond-TR visible absorption spectra of bR in the solution and the microcrystal upon photoexcitation at 532 nm. The figure illustrated the difference spectra, which were constructed by subtracting the dark state (bR570) spectrum from each TR spectrum. Here, the negative difference signal arose from bR570. The TR spectra of bR solution showed K590, L550, M412, and O640 intermediates in the photocycle, as previously reported [29]. The N560 intermediate did not significantly accumulate under the condition used (pH 5.5) [30]. The TR spectra of bR microcrystal showed no red-shifted peaks corresponding to K590 and O640. The global fitting analysis revealed that, in the microcrystal, L550 appeared within the current time resolution (<1 µs) and it was converted to M412 with a half-life time of 15 µs [7]; bR570 was then recovered with a half-life time of 8 ms, without the accumulation of O640, probably because the crystal packing affected the rate-limiting step of the reaction. However, it is known that an initial proton pump step after the retinal photoexcitation occurred during the transition of L550 to M412, accompanied by deprotonation of the retinal. Therefore, L550 and M412, as well as early K590 (<1 µs), were focused on in the TR-SFX experiment based on the TR spectroscopic results. These spectroscopic results on bR microcrystals underline the fact that TR-SFX should be used in combination with in crystallo TR spectroscopy. So far, in crystallo TR X-ray emission spectroscopy [31] and in crystallo TR-IR spectroscopy [32] have also been successfully combined to TR-SFX. Such combinatorial use of various TR spectroscopies, including Raman scattering, fluorescence, electron spin resonance, and so on, should be increasingly applied.

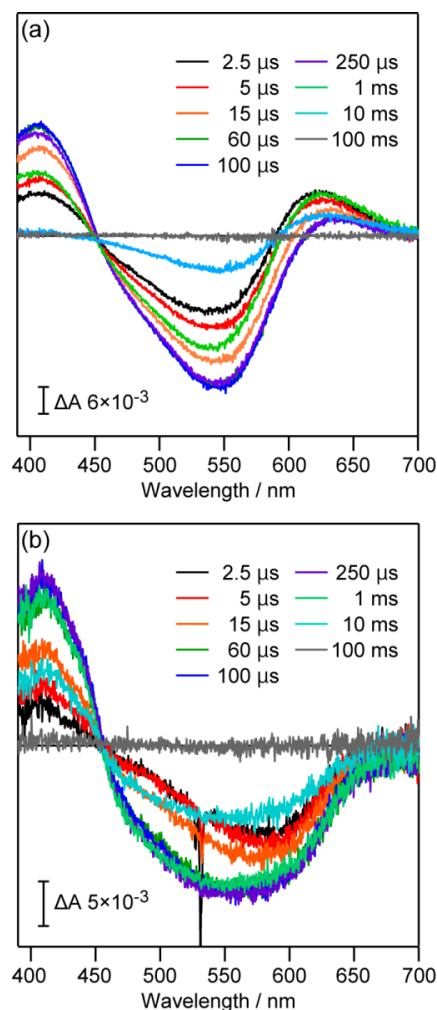


Figure 3. Time-resolved (TR) UV-visible spectra of bR in (a) a solution and (b) a microcrystal.

4. Data Collection Strategy for Pump-Probe TR-SFX Using a Highly Viscous Sample

In the following section, the experimental protocol of pump-probe TR-SFX while using our optical-fiber-based setup with the OPO pump-laser system will be described, which might aid in efficiently conducting TR-SFX experiments. We first focused on the technical matters on pump illumination, such as the pump pulse energy, pump pulse repetition rate, pump focal size, and the sample flow rate, as the actual experimental design and conditions, particularly pump illumination conditions, may be challenging to establish.

In crystallo TR spectroscopy should ideally determine the pump pulse energy at the sample point prior to TR-SFX experiments. In the TR-SFX study of bR, the pump energy was 4 μ J (2 μ J from each direction) with a \varnothing 40- μ m (FWHM) focal size, which was sufficient for the photoexcitation of the retinal in bR and it was below the threshold of sample damage by the pump pulse illumination. So far, the pump pulse energy used for TR-SFX was a few nJ/ μ m² or less [7–9].

The pump pulse repetition rate is adjustable to be sub-multiple of 30 Hz, which is the XFEL repetition rate at SACLA. Normally, the pump pulse repetition rate is chosen to be 10 or 15 Hz. At a 15-Hz pump repetition rate, a diffraction pattern from a non-illuminated crystal (“Dark”) is obtained at 33.3 ms after a diffraction pattern from a pump-illuminated crystal (“Light”) is recorded. The “Dark” image is useful for the calculation of $F_o(\text{“Light”}) - F_o(\text{“Dark”})$ difference Fourier maps for capturing protein conformational changes. At a 10-Hz pump repetition rate, a “Light” image, followed by two “Dark” images (“Dark1” at 33.3 ms and “Dark2” at 66.6 ms after the pump illumination), are sequentially obtained. Here, it should be noted that the sample flow rate has to be fast enough to

exchange pump-illuminated crystals with non-illuminated crystals within 33.3 or 66.6 ms for the 15- or 10-Hz pump repetition conditions, respectively, to obtain the “Dark” images. A detail of the suitable sample flow rate will be described later.

The pump focal size is adjustable from 20 to 250 μm , while using different core size optical fibers. The best pump focal size depends on delay times (Δt) of interest. Basically, for TR-SFX measurements with $\Delta t < \sim 1$ ms, the suitable pump focal size is about the diameter of the sample stream. However, for TR-SFX measurements with $\Delta t > \sim 1$ ms, the pump focal size should be larger because the pump-illuminated crystals move significantly downstream during the period of Δt . For example, the pump focal size was $\varnothing 40$ μm in FWHM ($\varnothing 90$ μm in full width) in the TR-SFX experiments for bR crystals with $\Delta t < 1$ ms (sample flow rate of 9.4 $\mu\text{m}/1$ ms) [7], whereas the pump focal size was set to be $\varnothing 250$ μm in TR-SFX experiments of P450nor with $\Delta t = 20$ ms (sample flow rate of 4.6 $\mu\text{m}/1$ ms) [9], where pump-illuminated crystals move approximately 90 μm downstream within 20 ms. The large pump focal size of $\varnothing 250$ μm allowed for crystals irradiation in the sample stream between the intersection point with XFEL and the position approximately 90- μm upstream from it, which ensured the integrity of ‘Light’ data collection without being influenced by the sample flow fluctuation. The stability of the sample speed would be required so that a pump-illuminated crystal can interact with XFEL after a certain delay time if the pump focal area was set to be well upstream and distant from the intersection point with XFEL. In TR-SFX of P450nor, the center of pump focal area was only aligned 45- μm upstream from the XFEL beam (3×3 μm^2), to secure the interaction of illuminated crystals with XFEL (Figure 4).

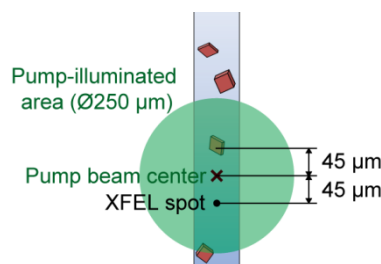


Figure 4. Spatial alignment of the pump-illuminated area.

The sample flow rate in pump-probe TR-SFX should be sufficiently fast for the “Dark” data collection to exchange the photoexcited crystals to the dark state crystals within 33.3 or 66.6 ms, while a sufficiently slow rate is needed for the “Light” data collection to ensure the interaction of the photoexcited crystals with an XFEL pulse. In the TR-SFX of bR experiments, the microcrystals in LCP were extruded at a flow rate of 2.5 $\mu\text{L}/\text{min}$. (9.4 $\mu\text{m}/1$ ms) from a nozzle of 75- μm internal diameter under the pump energy and size conditions that are mentioned above. Empirically, a sample flow rate of 5–10 $\mu\text{m}/1$ ms might be a good first choice for the design of more detailed experimental conditions. It should be noted that the pump-light scattering from the sample stream could pre-excite the sample being upstream. Therefore, care should be taken on the “Dark” data collection. A sample flow rate of >10 $\mu\text{m}/1$ ms might be needed, depending on the pump pulse energy and focal size. A 10-Hz pump repetition condition is a better choice than a 15-Hz condition in terms of the “Dark” data collection. The 10-Hz condition provides a sample exchange time of 66.6 ms, which is twice as long as the 15 Hz condition (33.3 ms). Thus, the sample flow rate can be reduced for the 10-Hz condition, which is twice as slow as for the 15-Hz condition.

With the above technical points in mind, in the XFEL beamtime, we performed the pump-probe TR-SFX according to the following protocol:

1. The data processing pipeline [33], which was based on Cheetah [34], was used for real-time feedback during the beamtime, hit finding, and sorting of “Light” and “Dark” images. In the pump-laser setup, a portion of the pump beam ($\sim 5\%$) was picked off and its intensity signal that was detected by a photodiode was used to tag the image as “Light”.

2. Protein microcrystals that were embedded in the carrier media were injected to the X-ray beam interaction point while using the high-viscosity sample injector [21]. The stability of the sample streams was essential for pump-probe TR-SFX experiments, because the pump-illuminated crystals must be exchanged with the fresh ones before the “Dark” data collection.
3. The injector height was aligned by using the sample stage (Z direction), so that the injector bottom was distant to the XFEL focal point by 300 μm . The monitor image of Microscope 1 was helpful (Figure 1) for the alignment.
4. The sample stream was aligned to the XFEL focal point by using the sample stage (X direction). The monitor image of Microscope 1 was also helpful for this alignment. The hit rate was maximized in the best alignment.
5. The sample stream was aligned to the pump focal area by using the sample stage (Y direction). The monitor image of Microscope 2 was helpful in this alignment (Figure 1). In the best alignment, the pump-light scattering from the sample stream was maximized.
6. The delay time (Δt) between the pump and XFEL pulses, which is controlled by a pulse generator (DG645, Stanford Research Systems), was set. The timing jitter for $\Delta t < 16.7$ ms was < 1 ns, but it was approximately 0.1 ms for $\Delta t > 16.7$ ms at SACLA.
7. Diffraction images were collected: typically, the hit rate of highly viscous samples is 20–30% by adjusting the crystal density to avoid multiple hits. 10,000–15,000 diffraction patterns are collected as hit “Light” images in an hour in the case of the 15-Hz pump laser condition. Given the typical indexing rate of 60–70%, 6000–10,000 indexed images are obtained in an hour. Because ~20,000 indexed images are needed to clearly visualize the differences between “Light” and “Dark”, one dataset takes 3–4 h, including the time for sample replenishment.
8. Measurement was repeated by using different values of Δt to afford a molecular movie.

5. Conclusions

We reviewed the historical background of pump-probe TR-SFX and the development of an optical-fiber-based setup for nanosecond pump-probe TR-SFX. The setup, which can provide various pump wavelengths from UV to near-IR, is simple and easy-to-operate and, thus, allows for users to collect as much data as possible in limited beamtime. These were the reasons why it has been applied to various samples to provide new insights into understanding protein functions. However, cautious attention is required for the pump pulse energy, pump pulse repetition rate, pump focal size, and the sample flow rate, according to the appropriate experimental procedure, to obtain interpretable difference maps from pump-probe TR-SFX. Particularly, in crystallo TR spectroscopy serves to determine the pump pulse energy for photoexcitation. Moreover, the TR spectroscopy yields information regarding the reaction intermediates and timing in which the reaction occurs in crystals.

Author Contributions: E.N. and M.K. wrote the paper. All authors reviewed and critiqued the manuscript.

Funding: S.I. and K.T. acknowledge the financial support from the X-ray Free-Electron Laser Priority Strategy Program from the Ministry of Education, Culture, Sports, Science and Technology (MEXT). S.I. acknowledges the Platform Project for Supporting Drug Discovery and Life Science Research (Basis for Supporting Innovative Drug Discovery and Life Science Research (BINDS)) from Japan Agency for Medical Research and Development (AMED). JSPS KAKENHI (Grant Numbers: JP18H02394, JP19H03171, JP19H05781, and JP19H05784) and RIKEN Pioneering Project “Dynamic Structural Biology” partially supported this work.

Acknowledgments: We thank Richard Neutze and Jan Davidsson for discussions on time-resolved crystallography. We are grateful to Ayumi Yamashita for her technical assistance with Figure 2.

Conflicts of Interest: The authors declare no conflict of interest.

References

1. Moffat, K. Time-resolved macromolecular crystallography. *Annu. Rev. Biophys. Biophys. Chem.* **1989**, *18*, 309–332. [[CrossRef](#)] [[PubMed](#)]

2. Neutze, R.; Wouts, R.; van der Spoel, D.; Weckert, E.; Hajdu, J. Potential for biomolecular imaging with femtosecond X-ray pulses. *Nature* **2000**, *406*, 752–757. [[CrossRef](#)] [[PubMed](#)]
3. Chapman, H.N.; Fromme, P.; Barty, A.; White, T.A.; Kirian, R.A.; Aquila, A.; Hunter, M.S.; Schulz, J.; DePonte, D.P.; Weierstall, U.; et al. Femtosecond X-ray protein nanocrystallography. *Nature* **2011**, *470*, 73–77. [[CrossRef](#)] [[PubMed](#)]
4. Boutet, S.; Lomb, L.; Williams, G.J.; Barends, T.R.; Aquila, A.; Doak, R.B.; Weierstall, U.; DePonte, D.P.; Steinbrener, J.; Shoeman, R.L.; et al. High-resolution protein structure determination by serial femtosecond crystallography. *Science* **2012**, *337*, 362–364. [[CrossRef](#)] [[PubMed](#)]
5. Ishikawa, T.; Aoyagi, H.; Asaka, T.; Asano, Y.; Azumi, N.; Bizen, T.; Ego, H.; Fukami, K.; Fukui, T.; Furukawa, Y.; et al. A compact X-ray free-electron laser emitting in the sub-angstrom region. *Nat. Photonics* **2012**, *6*, 540–544. [[CrossRef](#)]
6. Emma, P.; Akre, R.; Arthur, J.; Bionta, R.; Bostedt, C.; Bozek, J.; Brachmann, A.; Bucksbaum, P.; Coffee, R.; Decker, F.J.; et al. First lasing and operation of an angstrom-wavelength free-electron laser. *Nat. Photonics* **2010**, *4*, 641–647. [[CrossRef](#)]
7. Nango, E.; Royant, A.; Kubo, M.; Nakane, T.; Wickstrand, C.; Kimura, T.; Tanaka, T.; Tono, K.; Song, C.; Tanaka, R.; et al. A three-dimensional movie of structural changes in bacteriorhodopsin. *Science* **2016**, *354*, 1552–1557. [[CrossRef](#)]
8. Suga, M.; Akita, F.; Sugahara, M.; Kubo, M.; Nakajima, Y.; Nakane, T.; Yamashita, K.; Umena, Y.; Nakabayashi, M.; Yamane, T.; et al. Light-induced structural changes and the site of O=O bond formation in PSII caught by XFEL. *Nature* **2017**, *543*, 131–135. [[CrossRef](#)]
9. Tosha, T.; Nomura, T.; Nishida, T.; Saeki, N.; Okubayashi, K.; Yamagiwa, R.; Sugahara, M.; Nakane, T.; Yamashita, K.; Hirata, K.; et al. Capturing an initial intermediate during the P450_{nor} enzymatic reaction using time-resolved XFEL crystallography and caged-substrate. *Nat. Commun.* **2017**, *8*, 1585. [[CrossRef](#)]
10. Levantino, M.; Yorke, B.A.; Monteiro, D.C.; Cammarata, M.; Pearson, A.R. Using synchrotrons and XFELs for time-resolved X-ray crystallography and solution scattering experiments on biomolecules. *Curr. Opin. Struct. Biol.* **2015**, *35*, 41–48. [[CrossRef](#)]
11. Aquila, A.; Hunter, M.S.; Doak, R.B.; Kirian, R.A.; Fromme, P.; White, T.A.; Andreasson, J.; Arnlund, D.; Bajt, S.; Barends, T.R.; et al. Time-resolved protein nanocrystallography using an X-ray free-electron laser. *Opt. Express* **2012**, *20*, 2706–2716. [[CrossRef](#)] [[PubMed](#)]
12. Tenboer, J.; Basu, S.; Zatsepin, N.; Pande, K.; Milathianaki, D.; Frank, M.; Hunter, M.; Boutet, S.; Williams, G.J.; Koglin, J.E.; et al. Time-resolved serial crystallography captures high-resolution intermediates of photoactive yellow protein. *Science* **2014**, *346*, 1242–1246. [[CrossRef](#)] [[PubMed](#)]
13. Pande, K.; Hutchison, C.D.; Groenhof, G.; Aquila, A.; Robinson, J.S.; Tenboer, J.; Basu, S.; Boutet, S.; DePonte, D.P.; Liang, M.; et al. Femtosecond structural dynamics drives the trans/cis isomerization in photoactive yellow protein. *Science* **2016**, *352*, 725–729. [[CrossRef](#)] [[PubMed](#)]
14. Barends, T.R.; Foucar, L.; Ardevol, A.; Nass, K.; Aquila, A.; Botha, S.; Doak, R.B.; Falahati, K.; Hartmann, E.; Hilpert, M.; et al. Direct observation of ultrafast collective motions in CO myoglobin upon ligand dissociation. *Science* **2015**, *350*, 445–450. [[CrossRef](#)] [[PubMed](#)]
15. Liang, M.; Williams, G.J.; Messerschmidt, M.; Seibert, M.M.; Montanez, P.A.; Hayes, M.; Milathianaki, D.; Aquila, A.; Hunter, M.S.; Koglin, J.E.; et al. The Coherent X-ray Imaging instrument at the Linac Coherent Light Source. *J. Synchrotron Radiat.* **2015**, *22*, 514–519. [[CrossRef](#)] [[PubMed](#)]
16. Tono, K.; Nango, E.; Sugahara, M.; Song, C.Y.; Park, J.; Tanaka, T.; Tanaka, R.; Joti, Y.; Kameshima, T.; Ono, S.; et al. Diverse application platform for hard X-ray diffraction in SACLA (DAPHNIS): Application to serial protein crystallography using an X-ray free-electron laser. *J. Synchrotron Radiat.* **2015**, *22*, 532–537. [[CrossRef](#)] [[PubMed](#)]
17. Sierra, R.G.; Batyuk, A.; Sun, Z.; Aquila, A.; Hunter, M.S.; Lane, T.J.; Liang, M.; Yoon, C.H.; Alonso-Mori, R.; Armenta, R.; et al. The Macromolecular Femtosecond Crystallography Instrument at the Linac Coherent Light Source. *J. Synchrotron Radiat.* **2019**, *26*, 346–357. [[CrossRef](#)]
18. Kubo, M.; Nango, E.; Tono, K.; Kimura, T.; Owada, S.; Song, C.; Mafune, F.; Miyajima, K.; Takeda, Y.; Kohno, J.Y.; et al. Nanosecond pump-probe device for time-resolved serial femtosecond crystallography developed at SACLA. *J. Synchrotron Radiat.* **2017**, *24*, 1086–1091. [[CrossRef](#)]

19. Kameshima, T.; Ono, S.; Kudo, T.; Ozaki, K.; Kirihaara, Y.; Kobayashi, K.; Inubushi, Y.; Yabashi, M.; Horigome, T.; Holland, A.; et al. Development of an X-ray pixel detector with multi-port charge-coupled device for X-ray free-electron laser experiments. *Rev. Sci. Instrum.* **2014**, *85*. [\[CrossRef\]](#)
20. Weierstall, U.; James, D.; Wang, C.; White, T.A.; Wang, D.; Liu, W.; Spence, J.C.; Bruce Doak, R.; Nelson, G.; Fromme, P.; et al. Lipidic cubic phase injector facilitates membrane protein serial femtosecond crystallography. *Nat. Commun.* **2014**, *5*, 3309. [\[CrossRef\]](#)
21. Shimazu, Y.; Tono, K.; Tanaka, T.; Yamanaka, Y.; Nakane, T.; Mori, C.; Terakado Kimura, K.; Fujiwara, T.; Sugahara, M.; Tanaka, R.; et al. High-viscosity sample-injection device for serial femtosecond crystallography at atmospheric pressure. *J. Appl. Crystallogr.* **2019**, *52*. [\[CrossRef\]](#) [\[PubMed\]](#)
22. Landau, E.M.; Rosenbusch, J.P. Lipidic cubic phases: A novel concept for the crystallization of membrane proteins. *Proc. Natl. Acad. Sci. USA* **1996**, *93*, 14532–14535. [\[CrossRef\]](#) [\[PubMed\]](#)
23. DePonte, D.P.; Weierstall, U.; Schmidt, K.; Warner, J.; Starodub, D.; Spence, J.C.H.; Doak, R.B. Gas dynamic virtual nozzle for generation of microscopic droplet streams. *J. Phys. D Appl. Phys.* **2008**, *41*, 19. [\[CrossRef\]](#)
24. Nogly, P.; Panneels, V.; Nelson, G.; Gati, C.; Kimura, T.; Milne, C.; Milathianaki, D.; Kubo, M.; Wu, W.; Conrad, C.; et al. Lipidic cubic phase injector is a viable crystal delivery system for time-resolved serial crystallography. *Nat. Commun.* **2016**, *7*, 12314. [\[CrossRef\]](#)
25. Sugahara, M.; Mizohata, E.; Nango, E.; Suzuki, M.; Tanaka, T.; Masuda, T.; Tanaka, R.; Shimamura, T.; Tanaka, Y.; Suno, C.; et al. Grease matrix as a versatile carrier of proteins for serial crystallography. *Nat. Methods* **2015**, *12*, 61–63. [\[CrossRef\]](#)
26. Sugahara, M.; Nakane, T.; Masuda, T.; Suzuki, M.; Inoue, S.; Song, C.; Tanaka, R.; Nakatsu, T.; Mizohata, E.; Yumoto, F.; et al. Hydroxyethyl cellulose matrix applied to serial crystallography. *Sci. Rep.* **2017**, *7*, 703. [\[CrossRef\]](#)
27. Togashi, T.; Sato, T.; Ogawa, K.; Katayama, T.; Owada, S.; Inubushi, Y.; Tono, K.; Yabashi, M. Arrival-timing diagnostics for pump-probe experiments in SACLA, using X-ray-induced optical transparency in GaAs. In Proceedings of the 19th International Conference on Ultrafast Phenomena, Okinawa, Japan, 7–11 July 2014. [\[CrossRef\]](#)
28. Mafune, F.; Miyajima, K.; Tono, K.; Takeda, Y.; Kohno, J.Y.; Miyauchi, N.; Kobayashi, J.; Joti, Y.; Nango, E.; Iwata, S.; et al. Microcrystal delivery by pulsed liquid droplet for serial femtosecond crystallography. *Acta Crystallogr. D Struct. Biol.* **2016**, *72*, 520–523. [\[CrossRef\]](#)
29. Zimanyi, L.; Keszthelyi, L.; Lanyi, J.K. Transient spectroscopy of bacterial rhodopsins with an optical multichannel analyzer. 1. Comparison of the photocycles of bacteriorhodopsin and halorhodopsin. *Biochemistry* **1989**, *28*, 5165–5172. [\[CrossRef\]](#)
30. Kouyama, T.; Nasuda-Kouyama, A.; Ikegami, A.; Mathew, M.K.; Stoeckenius, W. Bacteriorhodopsin photoreaction: Identification of a long-lived intermediate N (P, R350) at high pH and its M-like photoproduct. *Biochemistry* **1988**, *27*, 5855–5863. [\[CrossRef\]](#)
31. Fuller, F.D.; Gul, S.; Chatterjee, R.; Burgie, E.S.; Young, I.D.; Lebrette, H.; Srinivas, V.; Brewster, A.S.; Michels-Clark, T.; Clinger, J.A.; et al. Drop-on-demand sample delivery for studying biocatalysts in action at X-ray free-electron lasers. *Nat. Methods* **2017**, *14*, 443–449. [\[CrossRef\]](#)
32. Shimada, A.; Kubo, M.; Baba, S.; Yamashita, K.; Hirata, K.; Ueno, G.; Nomura, T.; Kimura, T.; Shinzawa-Itoh, K.; Baba, J.; et al. A nanosecond time-resolved XFEL analysis of structural changes associated with CO release from cytochrome c oxidase. *Sci. Adv.* **2017**, *3*, e1603042. [\[CrossRef\]](#) [\[PubMed\]](#)
33. Nakane, T.; Joti, Y.; Tono, K.; Yabashi, M.; Nango, E.; Iwata, S.; Ishitani, R.; Nureki, O. Data processing pipeline for serial femtosecond crystallography at SACLA. *J. Appl. Crystallogr.* **2016**, *49*, 1035–1041. [\[CrossRef\]](#) [\[PubMed\]](#)
34. Barty, A.; Kirian, R.A.; Maia, F.R.; Hantke, M.; Yoon, C.H.; White, T.A.; Chapman, H. Cheetah: Software for high-throughput reduction and analysis of serial femtosecond X-ray diffraction data. *J. Appl. Crystallogr.* **2014**, *47*, 1118–1131. [\[CrossRef\]](#) [\[PubMed\]](#)

